Int. J. Electrochem. Sci., 16 **(2021)** Article ID: 210741, doi: 10.20964/2021.07.39

International Journal of
ELECTROCHEMICAL
SCIENCE
www.electrochemsci.org

A Study of Molybdenum Coatings Underpotential Preparation in an Ionic Liquid System

Huazhen Cao, Zhizhou Yue, Huibin Zhang, Guangya Hou, Yiping Tang, Guoqu Zheng[*]

College of Materials Science and Engineering, Zhejiang University of Technology, Hangzhou 310014, China,
[*]E-mail: zhenggq@zjut.edu.cn

Received: 24 March 2021 / *Accepted:* 10 May 2021 / *Published:* 31 May 2021

Electrodeposition of refractory metals is a challenging issue in the electroplating field owing to their low reduction potential. Electrodeposition of molybdenum in $MoCl_5$-$BMIMPF_6$ by a cyclic scanning regime was introduced in this paper. Ni-Mo and Pt/Ni-Mo deposits were prepared by underpotential deposition to induce the bulk deposition of molybdenum. The coatings were observed and characterized by scanning electron microscopy (SEM), energy dispersive spectroscopy (EDS) and X-ray photoelectron spectroscopy (XPS). The electrochemical behavior of metallic molybdenum in ionic liquids was studied by cyclic voltammetry and chronoamperometry. The results show that the initial nucleation/growth process of molybdenum in $MoCl_5$-$BMIMPF_6$ follows three-dimensional progressive nucleation with diffusion-controlled growth, and the nucleation rate of molybdenum is slow in the ionic liquid system. The effects of supporting electrolytes and sputtering Pt/Ni electrodes were particularly studied. A yellow-brown uniform coating with more refined crystalline grains was obtained on the Ni surface by the addition of NaF due to its positive role in the mass transfer process and good complexing actions that promote nucleation. A gray-white coating with metallic luster was successfully fabricated on the surface of sputtered Pt/Ni because the substrate with a high work function is benign to molybdenum growth at a lower temperature and more positive potentials.

Keywords: Molybdenum electroplating, ionic liquid, underpotential induced, supporting electrolyte, sputtering Pt

1. INTRODUCTION

Molybdenum is a silver-white refractory metal with many excellent properties including wear resistance, corrosion resistance, high hot strength, high hardness, high melting point, etc., which makes it widely used in modern science and engineering [1–6]. The application of molybdenum coatings is one of the most popular corrosion protection methods and the enhancement of wear resistance and surface hardness of materials.

The current approach to preparing molybdenum coatings primarily focuses on plasma spraying [7] and chemical vapor deposition [8] in industry. However, these methods generally require high temperatures and high energy consumption and bring a certain degree of environmental pollution at the same time. Electrodeposition is a mature technology for preparing metal coatings, while for some oxyphilic metals including Cr, Re, Mo, etc., electrodeposition process is usually more difficult, and the current efficiency is low. Especially for molybdenum galvanic coatings, it is generally challenging to fabricate from aqueous solutions since it has a high overpotential for molybdenum reduction and a low overpotential for hydrogen evolution. Specifically, the molybdenum plating process would be accompanied by a violent hydrogen evolution reaction. Many studies have shown that the hydrogen evolution reaction is more likely to occur than metal ion reduction [9], and molybdenum is more likely to combine with oxygen.

Therefore, the electrolyte system is a crucial factor for the fabrication of molybdenum galvanic coatings. Some researchers have prepared thin molybdenum deposits by electrodeposition in aqueous solutions with high concentrations of acetic acid [10,11], hydrofluoric acid [12] and citric acid [13], but the deposits were insufficient to protect the substrate. Compared with aqueous solutions, thick and uniform molybdenum deposits can be electrodeposited in molten salts [14–16]. The addition of fluoride ions to molten salt not only improved the adhesion of coatings but also increased the thickness of deposits and reduced the number of microcracks [17]. However, this process was accompanied by high temperature, high energy consumption, toxic gas, and equipment corrosion.

The ionic liquid is a potential solvent composed of ions that is liquid at room temperature. It is characterized by good electrical conductivity, difficulty in volatilization and combustion, stable electrochemical properties, and a much larger potential window. In recent years, an increasing number of researchers have attempted to electrodeposit refractory metals such as tantalum [18], niobium [19], zirconium [20], and titanium [21] in ionic liquids, but only a few studies have involved molybdenum electrodeposition [22]. The deposition potential of refractory metals in ionic liquids is negative, leading to ionic liquid instability after long-term use. The cyclic scanning regime can provide a deposition process from the initial peak potential to the reduction peak potential. Therefore, cyclic scanning electrodeposition in ionic liquids is a prospective approach to prepare refractory metals.

This research focuses on the cyclic scanning electrodeposition, electrochemical behavior and electrocrystallization of metallic molybdenum in $MoCl_5$-$BMIMPF_6$ and explores the effects of temperature, supporting electrolytes (NaCl, Na_2SO_4, LiF, NaF), and sputtering Pt/Ni electrodes on the coatings.

2. EXPERIMENTAL

$BMIMPF_6$ (purity>99%) ionic liquids were purchased from Lanzhou Chloride Institute and vacuum dried at 80 °C for 24 h before use to remove water. $MoCl_5$ (99.6%) was purchased from Aladdin and used without any treatment. 0.15 M $MoCl_5$ and 0.25 M supporting electrolyte were added to $BMIMPF_6$ and stirred for 5 h. All electrolytes were prepared under an argon atmosphere with a water and oxygen content less than 1 μL/L.

Cyclic scanning electrodeposition, and cyclic voltammetry, and chronoamperometry measurements were performed on a CHI660C Electrochemical Workstation. A three-electrode system was applied in this study with a Pt filament (0.06 mm × 30 mm, 99.99%) as the quasi-reference electrode. During electrodeposition, Ni plates (10 mm ×5 mm × 0.2 mm, 99.99%) or Ni plate-sputtered Pt was utilized as the working electrode, and Mo plates (25 mm × 20 mm × 0.25 mm, 99.99%) were used as the auxiliary electrode, with a scanning range from -1.0 V to -2.8 V and scan rate of 10 $mV \cdot s^{-1}$. Before electrodeposition, Ni plates and Mo plates were polished and ultrasonically cleaned with acetone and anhydrous ethanol and dried in cold air. After electrodeposition, all samples were cleaned with acetone, ethanol, and deionized water in turn and then dried by cold air. In cyclic voltammetry and chronoamperometry measurements, a Ni electrode (φ=3 mm) and Pt plates (25 mm × 25 mm × 0.2 mm, 99.99%) were used as the working electrode and auxiliary electrode, respectively.

Scanning electron microscopy (SEM, GeminiSEM 500) was used to observe the morphology of molybdenum deposits, and energy dispersive spectroscopy (EDS, GENESIS-4000) was used to analyze its composition. X-ray photoelectron spectroscopy (XPS, Thermo Scientific K-Alpha) was applied to determine the valence state of the elements in the coatings.

3. RESULTS AND DISCUSSION

3.1 Electrodeposition of molybdenum in $MoCl_5$-BMIMPF$_6$

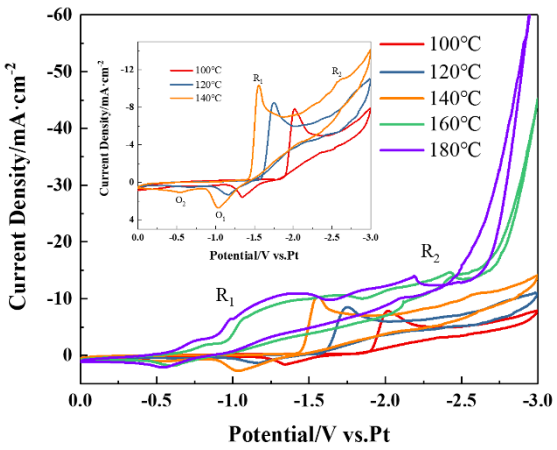

Figure 1. Cyclic Voltammograms in BMIMPF$_6$ with electrolyte of 0.15 M $MoCl_5$ under different temperatures, measured at scanning rate of 50 $mV \cdot s^{-1}$.

Typical CV curves of the Ni electrode in $MoCl_5$-BMIMPF$_6$ under different temperatures are displayed in Fig. 1. There were two reduction peaks (R_1, R_2) in the negative scanning and two oxidation peaks (O_1, O_2) in the back scanning. The current peaks R_1 and R_2 correspond to the reduction of Mo(V) to Mo(III) and Mo(III) to Mo(0), respectively. The oxidation peaks O_1 and O_2 are denoted as the oxidation of Mo(0) to Mo(III) and Mo(III) to Mo(V) [23]. With increasing temperature, the redox peaks

shift positively, and the peak current increases accordingly. The shape of the CV curve changes obviously at 160 °C due to the electrocrystallization nucleation of molybdenum. A current loop was observed between the anodic and cathodic current curves, which indicates the nucleation and growth process of molybdenum on the electrode surface [24]. According to the CV studies, the cyclic scan electrodeposition scanning range is determined from -1.0 V to -2.8 V.

The temperature has a significant effect on the electrodeposition process. It is essential to explore the effect of temperature on molybdenum electrodeposition to determine the optimal process. Fig. 2 shows the microstructure of samples in $MoCl_5$-$BMIMPF_6$ by cyclic scanning electrodeposition at different temperatures. No deposition was observed on the surface of the nickel substrate at electrolysis temperatures below 100 °C. A small number of granular deposits grew on the substrate by increasing the temperature, but this deposit layer could not prevent the nickel substrate from corrosion. When the temperature was increased to 160 °C, dense deposits were obtained that could efficiently inhibit surface corrosion. Upon further increasing the temperature to 180 °C, new small particles emerged on the dense electrodeposit layer, which caused the surface to become rougher. Metallic molybdenum is difficult to deposit on nickel substrates at low electrolysis temperatures. At higher temperatures, the diffusion rate of $MoCl_5$ increases as the ionic liquid viscosity decreases, and molybdenum is more easily deposited. However, the reduction reaction becomes too violent under high temperatures, which leads to clusters of particles grown on the deposited layer. However, it aggravates the corrosion of equipment and increases energy consumption. Therefore, the optimal temperature of electrodeposited molybdenum in $MoCl_5$-$BMIMPF_6$ is approximately 160 °C.

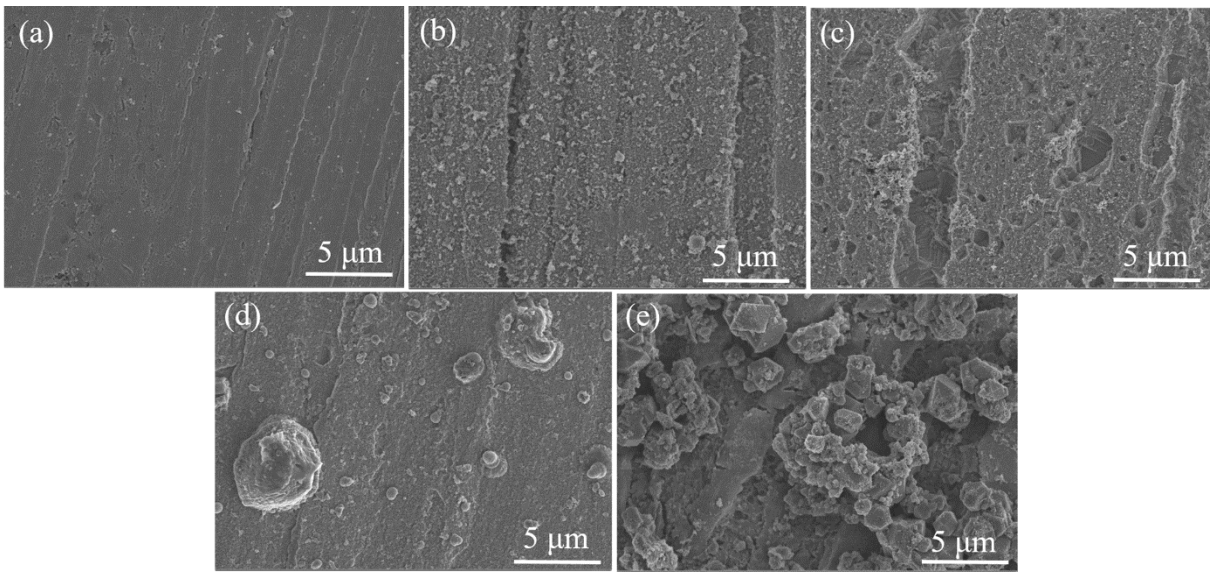

Figure 2. SEM images of coatings by cyclic scanning electrodeposition in $BMIMPF_6$ with electrolyte of 0.15 M $MoCl_5$ at temperatures of (a)100 °C, (b)120 °C, (c)140 °C, (d)160 °C, (e)180 °C (scanning range: -1.0 V~-2.8 V, scanning rate: 10 $mV \cdot s^{-1}$, deposition time: 5 h).

3.2 Nucleation mechanism in $MoCl_5$-BMIMPF$_6$

The above experiments showed that the electrochemical deposition rate of molybdenum in $MoCl_5$-BMIMPF$_6$ by cyclic electrodeposition was slow, so it is necessary to investigate the nucleation and growth mechanism in this system. Fig. 3a shows a set of voltammograms in $MoCl_5$-BMIMPF$_6$ obtained at different scan rates, and the fitting curves of E_p-ln$v$ and j-$v^{1/2}$ corresponding to reduction peak R_2 are presented in Fig. 3b and 3c. A linear relationship is detected between the peak potential (E_p) and the logarithm of the scanning rate (ln$v$). According to Laviron's theory, the reduction reaction of Mo is irreversible [25]. The control steps of electrochemical reactions are generally divided into electrode surface reaction control and diffusion mass transfer control. The linear relationship between the peak current density (j) and the square root of the scan rate ($v^{1/2}$) indicates that the reduction process of molybdenum is controlled by diffusion.

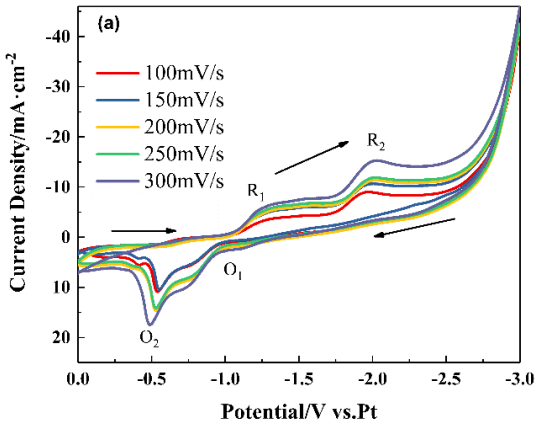

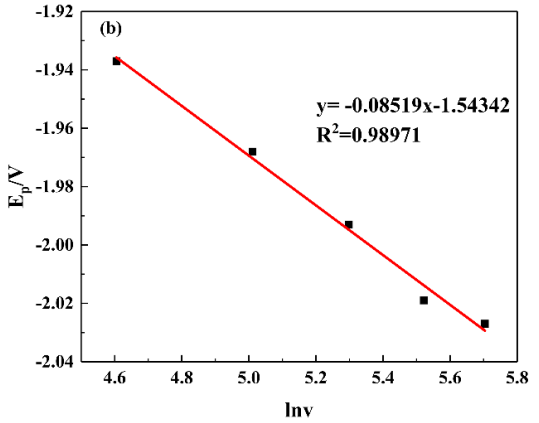

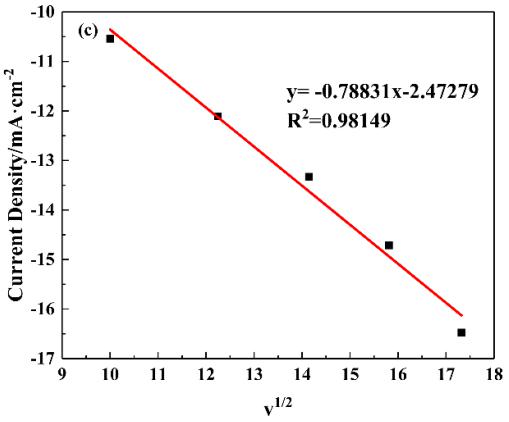

Figure 3. (a) Cyclic voltammograms of Ni electrode in $BMIMPF_6$ with electrolyte of 0.15 M $MoCl_5$ at 160 °C with different scanning rates, and the fitting curves of (b) E_p – ln$v$, (c) j-$v^{1/2}$ corresponding to the reduction peak R_2.

A family of potentiostatic current transients during molybdenum electrodeposition in $MoCl_5$-$BMIMPF_6$ electrolyte were recorded to investigate the nucleation process. Fig. 4a shows the current-time transient curves of $MoCl_5$-$BMIMPF_6$ from 0 steps to -1.8 V at 160 °C. First, double-layer charging occurred, and the current rose sharply and then fell to 110 mA·cm^{-2}. Then, the current rose to the maximum peak, and finally, the current decreased slowly. The curve does not correspond to a typical nucleation curve. The adsorption of defect sites on the electrode surface is parallel to nucleation/growth, so the time constant of initial transient current attenuation is much greater than the double layer's original charging current. Moreover, electrode surface absorption/desorption difficulty is due to the higher viscosity of ionic liquid than aqueous solutions. The charging current of the adsorption pseudocapacitor needs to be subtracted to study the electrocrystallization nucleation mechanism of molybdenum.

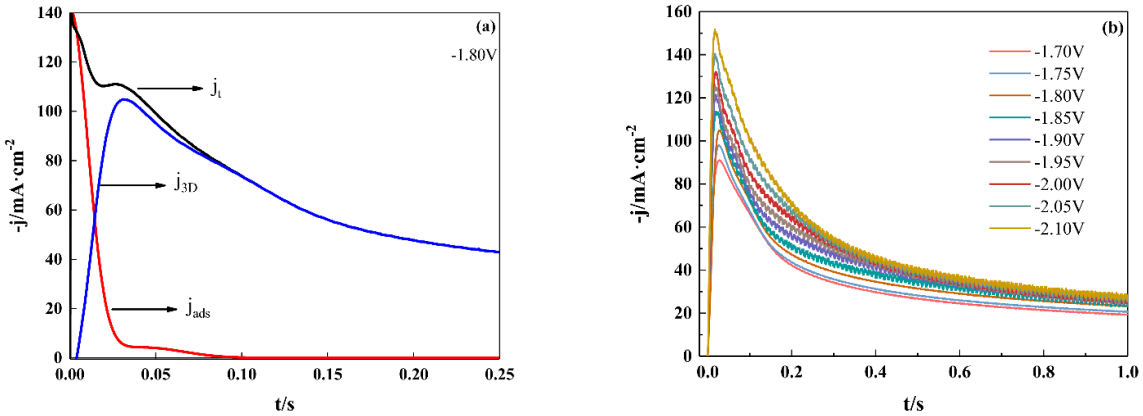

Figure 4. (a) Original, subtracted and double layer charging transients (j_t: the total current, j_{ads}: the adsorption current, j_{3D}: the nucleation current) and (b) subtracted current transients at different potentials in $BMIMPF_6$ with electrolyte of 0.15 M $MoCl_5$.

According to the studies of Barradas [26], Holzle [27], Romero-Romo [28], and Link [29], the adsorption current j_{ads} present a nonlinear relationship, as shown in formulas (3) and (4). After fitting,

the adsorption current can be calculated. The total current minus the adsorption current can be used to obtain the nuclear current, as shown in Fig. 4a. A typical nucleation process is when the current rises rapidly from 0 to the maximum value and then drops slowly. Fig. 4b shows the rectified nucleation curves from -1.70 V to -2.10 V. The nucleation peak current increased, and the nucleation time decreased as the step potential changed from -1.70 V to -2.10 V.

$$j_{3D} = \left[zFD^{1/2}c/\left(\pi^{1/2}t^{1/2}\right)\right]\{1 - exp\left[-N_0\pi kD\left(t - \left(1 - exp(-At)\right)/A\right)\right]\} \quad (1)$$

$$k = (8\pi cM/\rho)^{1/2} \quad (2)$$

$$j_{ads} = aq_{ads}exp(-at)^n \quad (3)$$

$$\mathrm{a} = k_a^0 exp\left[-(1-\beta)\frac{nFE}{RT}\right] = k_d^0 exp\left(\frac{\beta nFE}{RT}\right) \quad (4)$$

$$j_t = j_{3D} + j_{ads} \quad (5)$$

In formulas (1)-(5), j_{3D}[A·cm^{-2}] is the 3D nucleation current density, z is the number of transferred electrons, F[C·mol^{-1}] is the Faraday constant, c[mol·cm^{-3}] is the electrolyte concentration, t[s] is the time, N_0[cm^{-2}] is the total density of active sites, A[s^{-1}] is the nucleation rate of each active site, k is the growth rate of the diffusion zone, D[cm^2·s^{-1}] is the diffusion coefficient, M[g·mol^{-1}] is the molar mass, ρ[g·cm^{-3}] is the density, q_{ads} is the total charge of the adsorption process, k_a^0 and k_d^0 are the growth rates of the adsorption and desorption processes, respectively, R[J·mol^{-1}·K^{-1}] is the molar gas constant, and j_t[A·cm^{-2}] is the total current density.

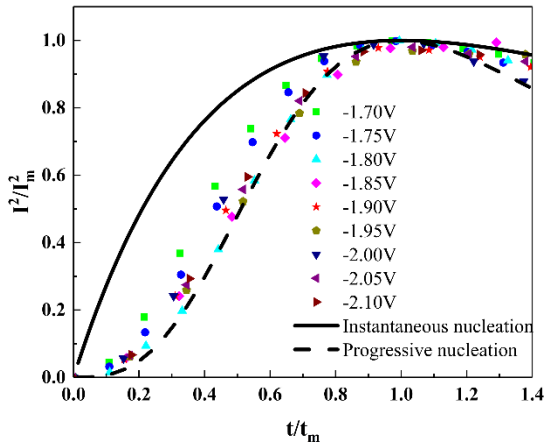

Figure 5. 3D dimensionless nucleation curves at different potentials in $BMIMPF_6$ with electrolyte of 0.15 M $MoCl_5$.

Sharifker et al. [30,31] proposed a three-dimensional nucleation model under diffusion control. The current density-time expression can be divided into two limit cases of instantaneous nucleation and continuous nucleation: in the first case, the nucleation rate is very high, and in the latter case, the nucleation rate has a low value [32]. The dimensionless expression can be obtained after differential transformation:

$$\frac{J^2}{J_m^2} = 1.9542/(t/t_m)\{1 - exp[-1.2564(t/t_m)]\}^2 \quad (6)$$

$$\frac{J^2}{J_m^2} = 1.2254/(t/t_m)\{1 - exp[-2.3367(t/t_m)^2]\}^2 \quad (7)$$

Fig. 5 displays the dimensionless curve of three-dimensional nucleation after fitting. The dimensionless curves obtained from the experimental data are approximate to continuous nucleation theoretical curves, which indicates that the nucleation rate of molybdenum in this system is slow. That is, the main factor limiting Mo electrodeposition is the process of crystal nucleus formation.

Based on the study of nucleation kinetics, it is necessary to take effective measures, for example, by regulating the composition of electrolytes or modifying the substrate to increase the crystal nuclei density on the electrode surface and accelerate crystal nucleus formation.

3.3 Effect of supporting electrolyte on the electrodeposition of molybdenum

The supporting electrolyte is an essential component that does not participate in the electrochemical reaction but can promote the mass transfer process and benefit the electrodeposition process. Therefore, it has been widely used in electrodeposition and electrocatalysis [33]. In the field of electrodeposition, the addition of supporting electrolytes can control the crystal morphology [34,35] and inhibit side reactions [36,37], thus improving current efficiency. It is difficult to prepare excellent molybdenum metal by adding only the main salt $MoCl_5$. The electrodeposition process can be optimized by introducing supporting electrolytes.

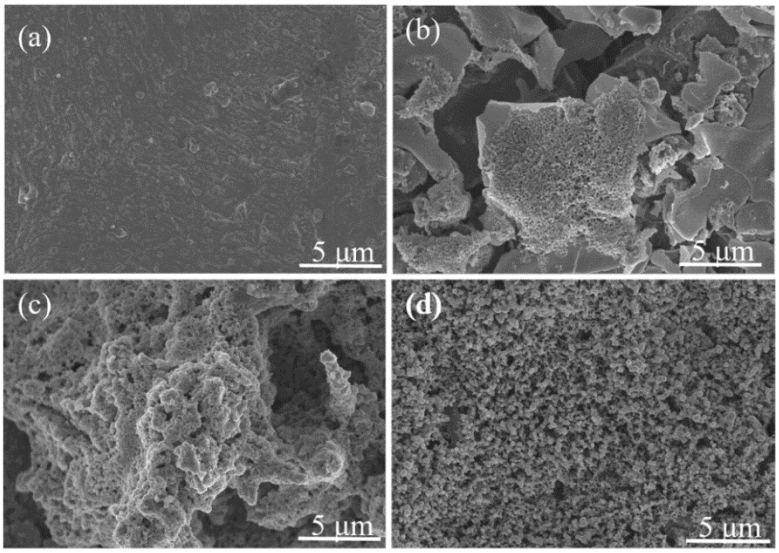

Figure 6. SEM images of electrodeposits by cyclic scanning electrodeposition in $BMIMPF_6$ with 0.15 M $MoCl_5$ and 0.25 M supporting electrolyte at 160 °C (scanning range: -1.0 V~ -2.8 V, scanning rate: 10 $mV \cdot s^{-1}$, deposition time: 5 h) (a) NaCl, (b) Na_2SO_4, (c) LiF, (d) NaF.

The supporting electrolyte is less soluble in ionic liquids. The supporting electrolyte is supersaturated to keep the electrolyte stable. In this paper, the supporting electrolyte concentration is 0.25 M. Fig. 6 shows the microstructure of samples prepared in $MoCl_5$-$BMIMPF_6$ containing different supporting electrolytes. By adding NaCl, Na_2SO_4, LiF or NaF into ionic liquids, black muddy deposits, gray muddy deposits, gray uneven films and yellowish-brown uniform deposits were obtained. Homogeneous small globular deposits grow on the substrate after adding NaF. Compared with Fig. 2d,

the addition of NaF resulted in deposits with finer microstructures. This may be attributed to complexing actions caused by fluoride ions, which can promote nucleation and thus refine the crystalline grains.

Fig. 7 shows the CV curves of the Ni electrode in $MoCl_5$-$BMIMPF_6$ with 0.25 M NaF at different temperatures. Similarly, there are two main reduction peaks (R_1, R_2) and two main oxidation peaks (O_1, O_2). Compared with that of the $MoCl_5$-$BMIMPF_6$ system (Fig. 1), the peak potential was corrected after adding NaF at the same temperature. The addition of a supporting electrolyte can ameliorate the mass transfer condition and benefit the deposition of molybdenum.

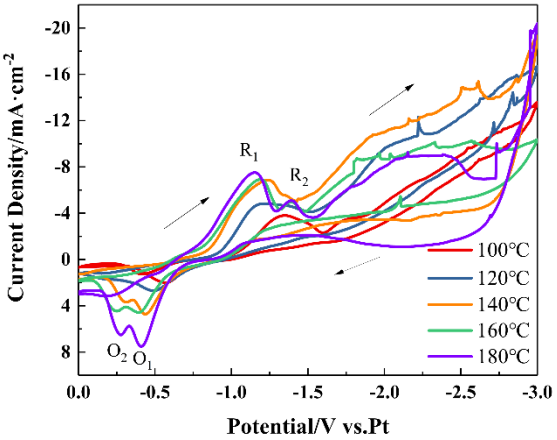

Figure 7. Cyclic Voltammograms in $BMIMPF_6$ with 0.15 M $MoCl_5$ and 0.25 M NaF under different temperatures, measured at scanning rate of 50 $mV \cdot s^{-1}$.

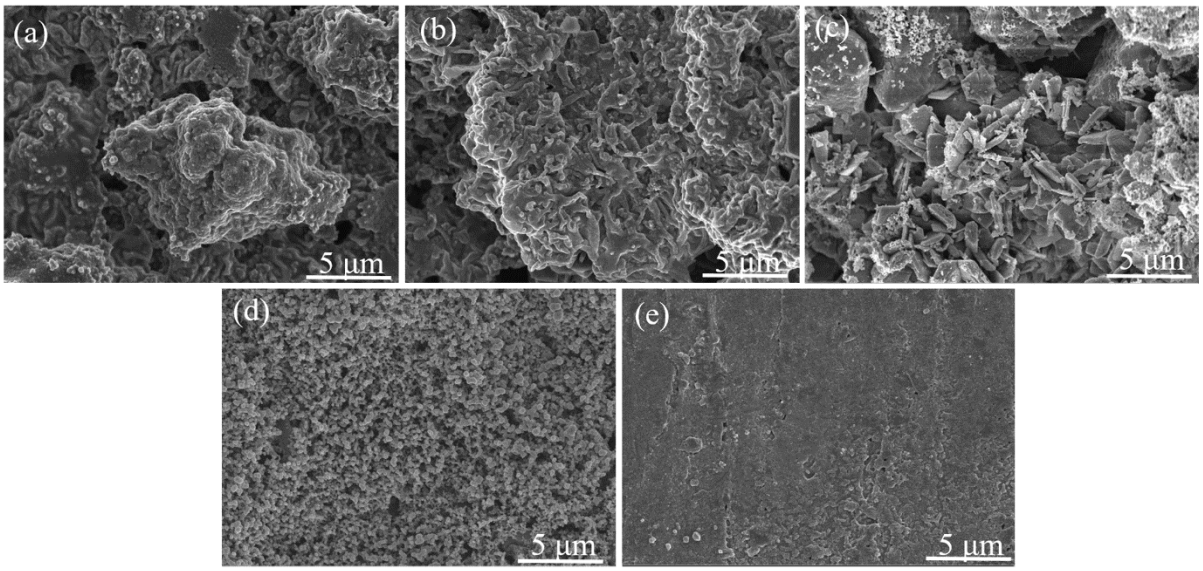

Figure 8. SEM images of electrodeposits by cyclic scanning electrodeposition in $BMIMPF_6$ with 0.15 M $MoCl_5$ and 0.25 M NaF at temperatures of (a)100 °C, (b)120 °C, (c)140 °C, (d)160 °C, (e)180 °C (scanning range: -1.0 V~-2.8 V, scanning rate: 10 $mV \cdot s^{-1}$, deposition time: 5 h).

Muddy deposits grew on the surface at 100-140 °C, while at 160 °C and 180 °C, the russet coating became compact. From the microscopic morphology shown in Fig. 8, as the temperature increases, the

deposited layer evolves from bulky clusters, strip clusters, mixed states, and uniform small microspheres to a dense structure.

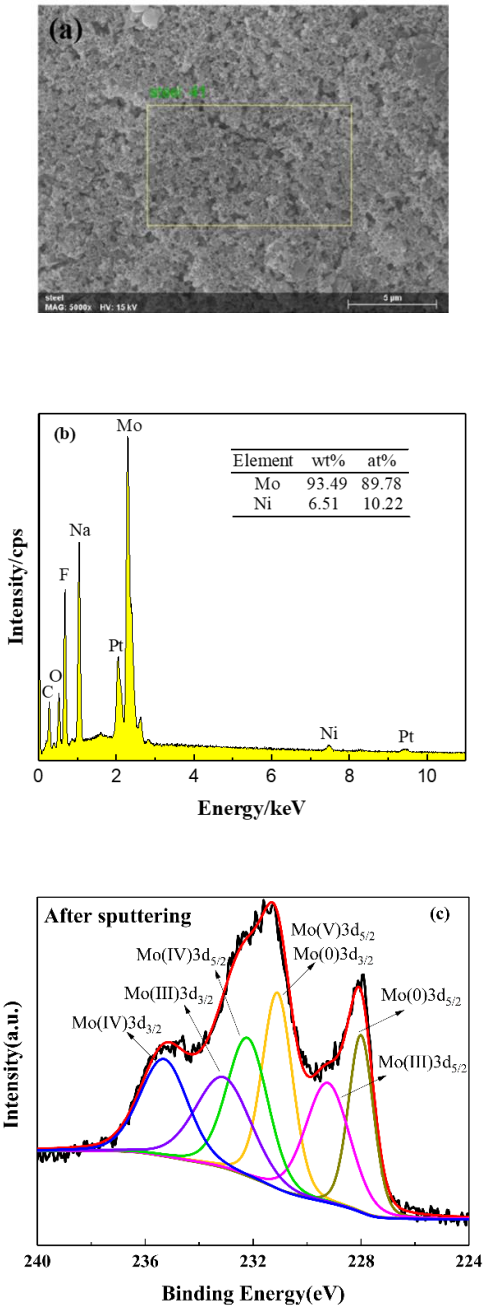

Figure 9. SEM image (a), corresponding EDS (b) and XPS (c) of the coating prepared by cyclic scanning electrodeposition in $BMIMPF_6$ with 0.15 M $MoCl_5$ and 0.25 M NaF at 160 °C (scanning range: -1.0 V~-2.8 V, scanning rate: 10 $mV \cdot s^{-1}$, deposition time: 5 h).

Combined with the results of macroscopic morphology and microscopic morphology, the optimal condition in the $MoCl_5$-$BMIMPF_6$-NaF system is cyclic scanning electrodeposition at 160 °C for 5 h. Fig. 9a and 9b are the scanning electron microscopy and the corresponding energy spectrum analysis diagrams of the optimal process. The C in the spectrum was from ionic liquid $BMIMPF_6$, O from oxygen

adsorption in the air, F from ionic liquid $BMIMPF_6$ and electrolyte NaF, Na from electrolyte NaF, Pt from sputter during electron microscopy, and the main element Mo accounted for 93.49 wt% relative to matrix element Ni. Fig. 9c is the XPS diagram of the deposit after 30 s of Ar^+ sputtering.

The results showed that the coating contained Mo(0), Mo(III), Mo(IV), and Mo(V). The two strongest peaks were $Mo(0)3d_{3/2}$ (231 eV) and $Mo(0)3d_{5/2}$ (228 eV). Mo(V) is caused by the attachment of the electrolyte $MoCl_5$ to the molybdenum layer. Mo(III) and Mo(IV) are intermediate products that have not been completely reduced. Therefore, it can be considered that the introduction of NaF into ionic liquid electrolytes is bound to have a positive effect on the electrodeposition of metallic molybdenum.

3.4 Effect of sputtering Pt/Ni electrode on the electrodeposition of molybdenum

Cyclic scanning electrodeposition includes underpotential deposition and bulk deposition. Underpotential deposition occurs when the work function of the substrate metal is greater than that of the deposited metal; that is, the more active metal deposits on the less active metal. The work function of Ni (4.6 eV) is higher than that of Mo (4.37 eV), so Mo could underpotential deposition on Ni. However, their work function difference is small, Mo adsorption on the nickel matrix is weak, and the nucleation rate is slow. Pt is an excellent electrodeposition substrate, and its work function (5.65 eV) is much higher than that of Mo and Ni. The adsorption of Mo ions on Pt is much higher than that on Ni, which could accelerate molybdenum nucleation. However, platinum is expensive, which is not conducive to industrial research. Via ion sputtering or electroless plating, and surface technologies, we can obtain an extremely thin Pt layer on the substrate and achieve the goal of improving the surface work function. In these experiments, sputtered Pt/Ni was used as the substrate to study molybdenum electrodeposition.

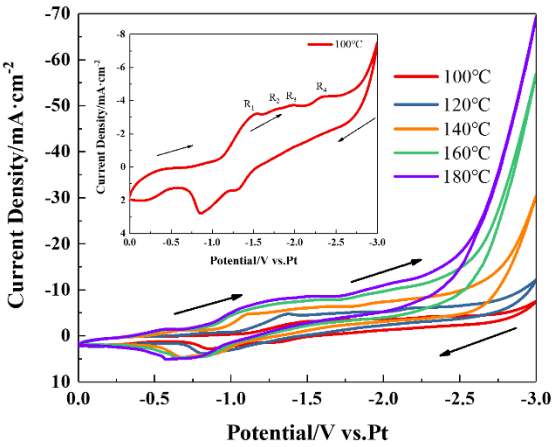

Figure 10. Cyclic Voltammogram in $BMIMPF_6$ with 0.15 M $MoCl_5$ on sputtering Pt/Ni under different temperatures, measured at scanning rate of 50 $mV \cdot s^{-1}$.

Characteristic CV curves of the sputtered Pt/Ni electrode in $MoCl_5$-$BMIMPF_6$ are presented in Fig. 10. As seen from the illustration, there are four reduction peaks in the potential range of -1.5 V~-

2.6 V at 100 °C. The number of reduction peaks is more significant than on the nickel electrode at 100 °C (Fig. 1), and the reduction peak potentials shift positively, showing that after sputtering Pt, Mo is more likely to be reduced on the electrode surface. This is attributed to the enhanced adsorption of molybdenum ions on the electrode surface by sputtering Pt. The mechanism of molybdenum reduction is more inclined to be the multistep single-electron reduction of Mo(V) [38]. With increasing temperature, the reduction peak current increases, and the reduction peak potential shifts positively, i.e., the temperature rise could promote molybdenum electrodeposition.

Fig. 11 illustrates the macroscopic observation of coatings by cyclic scanning electrodeposition in $MoCl_5$-$BMIMPF_6$ on nickel plates sputtered with platinum. Gray-white deposits with metallic luster were obtained at the studied temperatures. Under high temperatures (180 °C), the deposits on the edge of the electrode dissolve, bringing out a negative role instead.

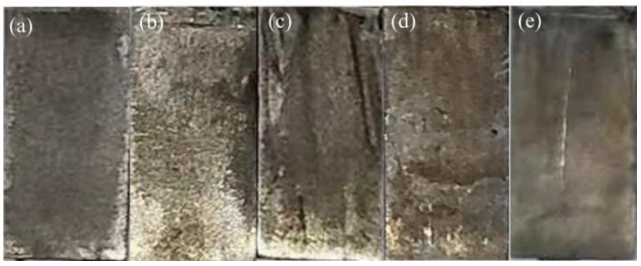

Figure 11. Images of coatings by cyclic scanning electrodeposition in $BMIMPF_6$ with 0.15 M $MoCl_5$ on nickel plates sputtered with platinum at temperatures of (a)100 °C, (b)120 °C, (c)140 °C, (d)160 °C, (e)180 °C (scanning range: -1.0 V~-2.8 V, scanning rate: 10 $mV \cdot s^{-1}$, deposition time: 5 h).

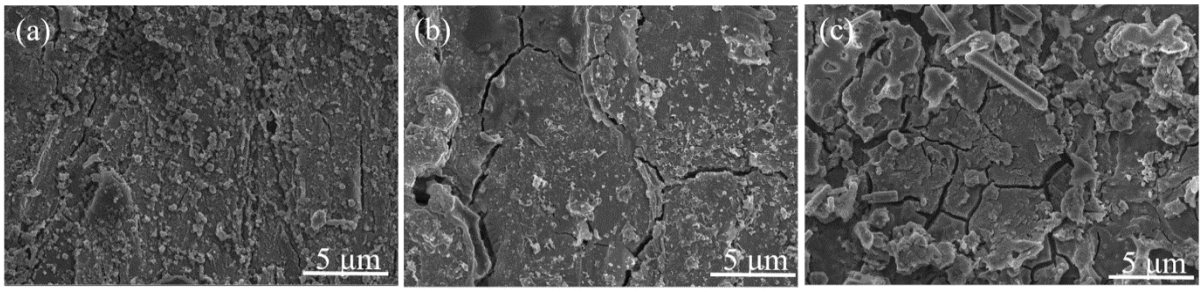

Figure 12. SEM images of electrodeposits by cyclic scanning electrodeposition in $BMIMPF_6$ with 0.15 M $MoCl_5$ on sputtering Pt/Ni at temperatures of (a)100 °C, (b)120 °C, (c)180 °C (scanning range: -1.0 V~-2.8 V, scanning rate: 10 $mV \cdot s^{-1}$, deposition time: 5 h).

The micromorphology of the molybdenum coating by cyclic electrodeposition on a Ni substrate with sputtered Pt is displayed in Fig. 12. A dense coating can be obtained at an electrolyte temperature of 100 °C, while cracks occur with increasing temperature. Serious spallation of the deposited layer was observed at 180 °C, due to the weakening of the bond between the deposited layer and the substrate at high temperatures. In this electrolysis system, chlorine evolution occurs during the anodic process, which usually easily causes cracks on coatings. A higher temperature aggravating side effects; therefore, the

optimal temperature for sputtering Pt/Ni substrates is approximately 100 °C because the deposited layer is more uniform and compact in this case. Compared with the reported literature [22], molybdenum can be deposited at a lower temperature on the surface of metals with a higher work function.

4. CONCLUSIONS

A novel approach for preparing molybdenum galvanic coatings from ionic liquid systems was introduced via cyclic scanning electrodeposition. The initial nucleation/growth process of molybdenum follows three-dimensional progressive nucleation with diffusion-controlled growth. The low nucleation rate on the Ni electrode is one main factor limiting molybdenum electrodeposition. Effective ways to improve molybdenum electrodeposition in $MoCl_5$-$BMIMPF_6$ are explored in this study. The mass transfer rate can be changed by adding supporting electrolytes. Dense and uniform molybdenum deposits were obtained at 160 °C by adding NaF to $MoCl_5$-$BMIMPF_6$, and Mo accounted for 93.49 wt% of the base element Ni. Modification of the Ni surface with high work function metals (e.g., Pt) can promote Pt/Ni-Mo layers growth at a lower temperature and more positive potentials, which is conducive to bulk deposition. This study provides a reference for the electrodeposition of refractory metals.

ACKNOWLEDGMENT
This work was financially supported by the National Natural Science Foundation of China (No. 51374185).

Reference

1. W.J. Zhang, J.T. Li, Z.W. Zhao and F. Li, *Trans. Nonferrous Met. Soc. China*, 26 (2016) 2731.
2. J.H. Perepezko, *Annu. Rev. Mater. Res.*, 45 (2015) 519.
3. A. Hosseinzadeh, M. Nazmabadi and N. Vosoughi, *Surf. Coatings Technol.*, 309 (2017) 1052.
4. B. Szczygieł, A. Laszczyńska and W. Tylus, *Surf. Coatings Technol.*, 204 (2010) 1438.
5. Z.N. Lou, Y.X. Li, F.Q. Ren, Q. Zhang, L. Wan, Z.Q. Xing, S.L. Zang and Y. Xiong, *Rare Met.*, 35 (2016) 502.
6. J.H. Ye, C.K. Cheng, J.Y. Lin, C.H. Huang, T.K. Yeh and C.K. Hsieh, *Surf. Coatings Technol.*, 394 (2020) 125855.
7. S. Sampath and S.F. Wayne, *J. Therm. Spray Technol.*, 3 (1994) 282.
8. S.T. Wlodek and J. Wulff, *J. Electrochem. Soc.*, 107 (1960) 565.
9. H.Z. Cao, C.J. Tong, H.B. Zhang and G.Q. Zheng, *Trans. Nonferrous Met. Soc. China*, 29 (2019) 1744.
10. S.N. Hasan, M. Xu and E. Asselin, *Surf. Coatings Technol.*, 357 (2019) 567.
11. A. Haftbaradaran, N. Parvini-Ahmadi and S. Yazdani, *Surf. Coatings Technol.*, 324 (2017) 1.
12. N.D. Ivanova, S. V. Ivanov, E.I. Boldyrev and O.A. Stadnik, *Prot. Met.*, 42 (2006) 354.
13. R. Syed, S.K. Ghosh, P.U. Sastry, G. Sharma, R.C. Hubli and J.K. Chakravartty, *Surf. Coatings Technol.*, 261 (2015) 15.
14. F.X. McCawley, C. Wyche and D. Schlai, *J. Electrochem. Soc.*, 106 (1959) 119.
15. H. Nakajima, T. Nohira and R. Hagiwara, *Electrochim. Acta*, 51 (2006) 3776.

16. G.J. Kipouros and D.R. Sadoway, *J. Appl. Electrochem.*, 18 (1988) 823.
17. S. Senderoff and G.W. Mellors, *J. Electrochem. Soc.*, 114 (1967) 556.
18. S. Krischok, A. Ispas, A. Zühlsdorff, A. Ulbrich, A. Bund, and F. Endres, *ECS Trans.*, 50 (2012) 229.
19. P. Giridhar, S. Zein El Abedin, A. Bund, A. Ispas and F. Endres, *Electrochim. Acta*, 129 (2014) 312.
20. A. Vacca, M. Mascia, L. Mais, F. Delogu, S. Palmas and A. Pinna, *Mater. Manuf. Process.*, 31 (2016) 74.
21. Q. Wu, G. Pulletikurthi, T. Carstens and F. Endres, *J. Electrochem. Soc.*, 165 (2018) D223.
22. X.T. Hu, J.G. Qian, Y. Yin, X. Li, T.J. Li and J. Li, *Rare Met.* (2018) 1.
23. D. Inman and S.H. White, *J. Appl. Electrochem.*, 8 (1978) 375.
24. H.Z. Cao, Y.F. Zhang, Q.Q. Wang, L.K. Wu and G.Q. Zheng, *Trans. Nonferrous Met. Soc. China*, 27 (2017) 2291.
25. W. Li, J. Hao, S. Mu and W. Liu, *Appl. Surf. Sci.*, 507 (2020) 144889.
26. R.G. Barradas and E. Bosco, *J. Electroanal. Chem.*, 193 (1985) 23.
27. M.H. Hölzle, U. Retter and D.M. Kolb, *J. Electroanal. Chem.*, 371 (1994) 101.
28. M. Romero-Romo, J. Aldana-González, L.E. Botello, M.G. Montes de Oca, M.T. Ramírez-Silva, S. Corona-Avendaño and M. Palomar-Pardavé, *J. Electroanal. Chem.*, 791 (2017) 1.
29. S. Link, S. Ivanov, A. Dimitrova, S. Krischok and A. Bund, *J. Cryst. Growth*, 531 (2020) 125346.
30. B. Scharifker, *Electrochim. Acta*, 28 (1982) 879.
31. B. Scharifker and J. Mostany, *J. Electroanal. Chem.*, 177 (1984) 13.
32. H.Z. Cao, D. Yang, S.L. Zhu, L. Dong and G.Q. Zheng, *J. Solid State Electrochem.*, 16 (2012) 3115.
33. P. Saxena and J. Ruparelia, *J. Inst. Eng. Ser. A*, 100 (2019) 299.
34. L. Wang, G. Liu and D. Xue, *Electrochim. Acta*, 56 (2011) 6277.
35. F.J. Vidal-Iglesias, R.M. Arán-Ais, J. Solla-Gullón, E. Herrero and J.M. Feliu, *ACS Catal.*, 2 (2012) 901.
36. J. Zambrano and B. Min, *Environ. Technol. Innov.*, 15 (2019) 100382.
37. H.Z. Cao, L.L. Hu, H.B. Zhang, G.Y. Hou, Y.P. Tang and G.Q. Zheng, *Int. J. Electrochem. Sci.*, 15 (2020) 6769.
38. J. Phillips and R.A. Osteryoung, *J. Electrochem. Soc.*, 124 (1977) 1465.